




Optimizing Laser Beam Welding Performance Parameters on Nimonic 80A Superalloy: A Study on Experimentation, TGRA, and PCA

Suman Kumar Saurabh¹ , Prabha Chand¹ , Umacharan Singh Yadav² 

¹ National Institute of Technology – NIT, Department of Mechanical Engineering, Jamshedpur, India.

² Ministry of Defence, Directorate General of Aeronautical Quality Assurance – DGAQA, Hindustan Aeronautic Ltd. – HAL, Kanpur, India.

How to cite: Saurabh SK, Chand P, Yadav US. Optimizing laser beam welding performance parameters on nimonic 80A superalloy: a study on experimentation, TGRA, and PCA. *Soldagem & Inspeção*. 2024;29:e2904. <https://doi.org/10.1590/0104-9224/SI29.04>

Abstract: This article describes the effect of CO₂ LBW performance parameters for the welded joint of 1.5 mm thin sheet of Nimonic 80A superalloy. Superalloy 80A used in high temperature application as aero-engine components- blade, rings, exhaust gas turbine part, nuclear tube support and automobile valve. The study focused on optimizing the welding process for the welded joints. Here, LP, WS, FD, and shielding GR will be optimised to improve the weld quality of Nimonic 80A material. Two different optimization techniques were used. The first method is SOO, which is based on the S/N ratio. The aim of this method is to find the Single-optimal values of process parameters. The second method employed MOO, combining the Taguchi grey relational analysis (TGRA) with the principal component analysis (PCA) technique. The researchers used these methods in an effort to identify the set of parameters for obtaining improved weld quality. Authors find best setting parameters $p_3-v_3-f_3-g_1$, with the specific parameter values are LP 2400 W, WS 1800 mm/min, FD 18 mm, and GR 10 lpm. The optimized parameters have yield significant improvements in the depth of penetration 6.03%, weld bead 8.74%, Vickers hardness 12.5%, and tensile strength 16.48% by using TGRA coupled with PCA.

Key-words: Nimonic 80A; CO₂ laser beam welding; Single-objective optimization; Multi-objective optimization; TGRA coupled with PCA.

1. Introduction

The article is endeavouring to discover and handle the input process parameters in order to generate high-quality weld joints that resemble the specified specifications. Traditional approaches including trial and error testing are used to determine welding parameter values. This approach is time-consuming, error-prone, and inefficient, leading to unreliable results. The aim of the present authors is to address this issue using a statistical method for optimizing process parameters.

The goal of optimization is to find the best set(s) of input (process) parameters, including LP, WS, FD, GR, among others. The study aims to lower different welding features such as weld bead width and heat-affected zone while concurrently enhancing joint attributes such as tensile strength, depth of penetration, microhardness, and others by optimising these parameters [1]. Researchers Huang et al. [2] have concentrated on selecting precise input parameters to accomplish high-quality welding in sheet metal using a CO₂ laser beam. LP, WS, focal location, and gas flow are among these characteristics. Similarly, Pankaj et al. [3] used CO₂ laser butt welding to evaluate the microstructure and mechanical characteristics of AISI304 steel and mild steel. They considered a variety of input factors, such as LP, WS, FD, and GR. The CO₂ LBW welding technique offers various advantages, including high precision, faster WS, reduced heat input, decreased post-weld processing, and improved overall quality when compared to manual arc welding. By CO₂ LBW, the authors aimed to harness these benefits and optimize the welding process parameters to achieve superior weld quality for their specific application.

The present researchers used Nimonic 80A superalloy. Nimonic 80A, a nickel-chromium superalloy, has excellent high-temperature strength, weldability, strength-to-weight ratio, and corrosion and oxidation resistance. These qualities make it ideal for many applications, As in aircraft engines, particularly in the combustion and turbine sections. High-performance materials are important in power generation and other industries [4,5]. Subramani et al. [6] compared GTAW and PCGTAW on Alloy 80A. PCGTAW enhanced joint quality over GTAW. In another study, Ancona et al. [7] compared two shielding gas delivery methods in autogenous laser beam welding (LBW) and examined how process parameters affect bead profile. The study found that travel speed was crucial to LBW, but gas flow rate and nozzle stand-off distance had no effect on penetration depth. Benyounis et al. [8] employed the Design Expert software and utilized the response surface method (RSM) to determine the optimal process parameters for CO₂ LBW of austenitic steel. The researchers created a mathematical model that included LP, WS, and focal position. The model incorporated output characteristics as tensile, impact, and joint operating cost. The authors

Received: 21 June, 2023. Accepted: 15 Jan., 2024.

E-mail: sksmech2012@gmail.com (SKS)



This is an Open Access article distributed under the terms of the Creative Commons Attribution license, which permits unrestricted use, distribution, and reproduction in any medium, provided the original work is properly cited.

aimed to cut costs while enhancing the cohesion of joints. Moradi and Ghoreishi's [9] analyzed the CO₂ LBW in nickel superalloy Rene 80. The research work focusing on the surface width, middle weld-bead width, and penetration. Using a statical RSM and mathematical equation to find that welding speed significantly affected on these parameters. It is noted that higher welding speed resulted in reduced surface width, middle weld-bead width, and penetration. Conversely, it has been observed that laser power exhibited a direct correlation with the welding properties, whereby an increase in laser power resulted in a corresponding rise in such features. Padmanaban and Balasubramanian [10] have established an empirical correlation to predict the tensile strength of a magnesium alloy often employed in laser beam welding (LBW). A three-factor, three-level, central composite face-centered design matrix and extensive replication were used in the trials. Researcher used RSM and Design Expert statistical software to optimise outcomes. Their investigation showed that welding speed significantly affects magnesium alloy tensile strength. Sathiyi et al. [11] tested laser-welded butt joints with argon, helium, and nitrogen shielding gases to determine tensile strength and bead profiles. The researchers used an extensive process that included the Taguchi method, grey relational analysis, and the desirability approach to get the best results and find the best welding settings for each shielding gas. The authors also analyzed to see how different parameters affected the success of welding with different shielding gases. Benyounis et al. [12] used response surface methodology to optimize laser welding's mechanical properties. Park and Rhee [13] studied how minor welding condition changes affected bead size and weld strength in a laser production line. Anawa and Olabi [14] analyzed and optimized CO₂ laser weld pool geometry using the Taguchi method, incorporating input variables. Choudhury et al. [15] optimized weld bead shape and strength. The hybrid optimization approach coupled a desire function with grey relational analysis (DFGRA). This method achieved all goals at once, resulting in an ideal weld parameter configuration of I3-V1-GFR2-N1. Increased welding current and lowered welding speed increased heat input, which improved weldment penetration and ultimate tensile strength. The Taguchi method, fuzzy logic, grey relational analysis (GRA), principal component analysis (PCA), and Technique for Order Preference by Similarity to Ideal Solution (TOPSIS) have been integrated to improve industrial process reliability and stability for high-quality welding results. These methodologies have been utilized to optimize a range of welding parameters, aiming to attain the optimal weld strength for diverse alloys and steel grades. The optimal solutions derived from these approaches have demonstrated noteworthy enhancements in process efficiency and product quality [16-20]. The optimal settings resulted in a 28.51% improvement in HAZ area and a 5.94% improvement in HAZ hardness. To improve the performance of electrical discharge machining, multi-criteria decision-making based on TGRA was used. Material removal rates, surface roughness, microhardness, and white layer thickness were evaluated. Peak current was found to have the greatest impact on performance measures. Payal et al. [21] reported multi-optimized input parameters for EDM of Inconel 825 using GRA coupled with PCA together, resulting in improved performance parameters [22]. Researchers working to reduce the heat-affected zone (HAZ) in welding, which is prone to cracking. They conducted experiments on micro-alloyed high-strength pipeline steel using submerged arc welding (SAW) with varying process factors. Response surface methodology (RSM) and grey relational analysis (GRA) were used to optimize HAZ characteristics (area and hardness). To eliminate correlations among the heat-affected zone (HAZ) characteristics, principal component analysis (PCA) was applied [23].

Based on the existing literature, and to the best of author's knowledge no prior reports have been found that utilize the combined approach of TGRA and PCA to optimize the laser welding process for the selected superalloy (Nimonic 80A) and its corresponding response variables. Therefore, this study aims to introduce a novel approach to optimize the laser welding process by identifying the foremost parameters for each response variable and simultaneously optimizing multiple responses. This approach has the potential to enhance the quality of the weld joint of the laser welding process for the superalloy. The aim of this paper is to assess and optimize the influence of laser welding parameters on different outcome variables concerning the Nimonic 80A superalloy. The combine Taguchi Grey relational analysis (TGRA) and principal component analysis (PCA) is used to achieve its objective. The author conducted nine experiments using a L9 Taguchi orthogonal array to discover the optimal combination of settings for four response variables in laser welding of superalloy. The response variables included weld bead width (BW), depth of penetration (DP), microhardness (HV), and tensile strength (TS). The research commences by discussing the selection process of material and process parameters, followed by the implementation of the Taguchi experimental design using Minitab statistical software version 20.3. The analysis of the experimental results involves the utilization of Taguchi signal-to-noise ratios, as well as the integration of GRA and PCA techniques. Finally, the experimental findings are validated through confirmatory experiments in the concluding section.

2. Materials and Methods of Experimentation

2.1. Weld Material

A gas turbine blade of Nickel base Superalloy Nimonic 80A of 1.5 mm thickness was square butt welded through CO₂ laser welding process. Their chemical composition is determined by the optical spark erosion method in Table 1.

Table 1. Nimonic 80A superalloy chemical composition (by weight%).

Elements	Cr	Al	Ti	Fe	Co	C	Si	Mn	Ni
Percentage	20	1.5	1.6	2.0	1.1	0.06	0.4	0.2	Bal.

2.2. Experimental setup and weld joint

To ensure precise and sharp edge cutting, the weld samples were cut using the wire-cut Electrical discharge machining process. Following the cutting process, the edges were cleaned with acetone and the oxide layer was removed using sandpaper before the welding process. A butt-joint configuration was employed to investigate the process parameters of CO_2 laser welding performance. The joint configuration was securely positioned on a fixture, ensuring a seamless edge alignment without any bends, gaps, or misalignments during the welding process. Figure 1 illustrates the laser welding setup, where the input parameters are transmitted to the numerical control unit. The experiment was carried out using various input parameters, namely LP, WS, FD, and shield GR (Ar gas), while maintaining a constant laser beam spot diameter.

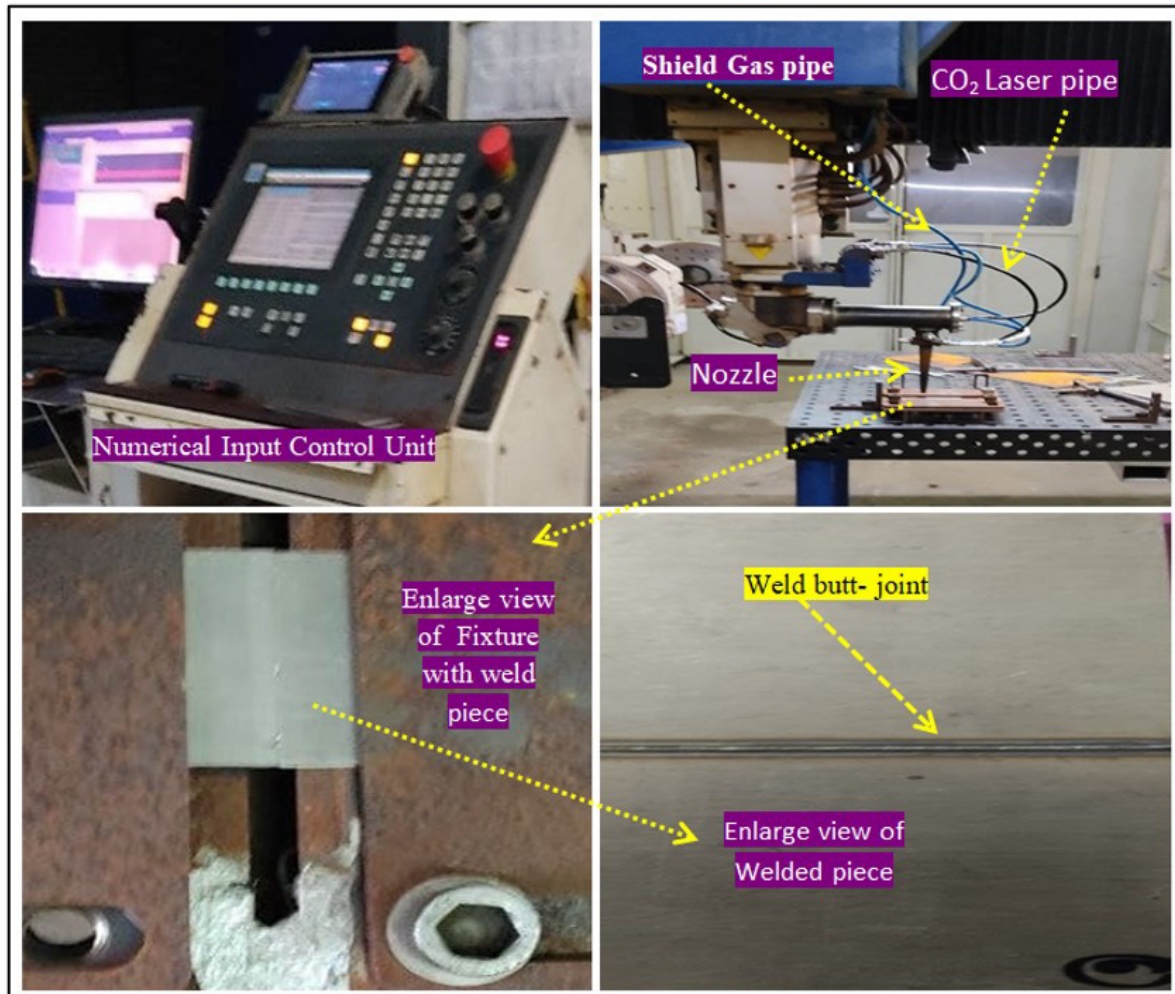


Figure 1. Experimental setup of CO_2 laser welding.

2.3. Input-process parameters

The input process parameters for CO_2 laser beam welding in this experiment were chosen through a comprehensive analysis of literature studies, machine capabilities, expert opinions from welding specialists, and exhaustive pilot experiments. The parameters selected were LP (p), WS (v), FD (f), and shield GR (g) due to their foremost impact on the quality of the weld joints. Table 2 presents the selected welding parameters, along with their corresponding units and levels.

Table 2. Welding parameters for welding and their level

Factors (Input parameters)	Symbol	Unit	Levels		
			1	2	3
Laser power	p	Watt	2000	2200	2400
Welding speed	v	mm/min	1400	1600	1800
Focal distance	f	mm	14	16	18
Gas flow rate	g	lpm	10	15	20

2.4. Response parameters

In the present article, the weld bead width (BW), depth of penetration (DP), microhardness (HV), and tensile strength (TS) were chosen as response parameters to evaluate the quality of the welded joints. Table 3 presents these response parameters, which were subsequently subjected to multi-optimization in order to determine the optimal welding process parameter that simultaneously meets the desired attributes of the weld joint.

Table 3. Design of experiments L_9 and response Parameters.

Exp.No	Coded OA				Uncoded OA				Experimental responses			
	p	v	f	g	p	v	f	g	DP	BW	HV	TS
1	1	1	1	1	1200	2000	14	10	1.824	1.589	256	716
2	1	2	2	2	1200	2200	16	15	1.670	1.673	263	736
3	1	3	3	3	1200	2400	18	20	1.618	1.743	292	817
4	2	1	2	3	1400	2000	16	20	1.604	1.743	248	694
5	2	2	3	1	1400	2200	18	10	1.610	1.809	280	784
6	2	3	1	2	1400	2400	14	15	1.540	1.655	240	672
7	1	1	1	1	1200	2000	14	10	1.824	1.589	256	716
8	1	2	2	2	1200	2200	16	15	1.670	1.673	263	736
9	1	3	3	3	1200	2400	18	20	1.618	1.743	292	817

2.4.1. Depth of penetration (DP)

The macrostructure of CO_2 laser welded joints was examined using an optical microscope (OM) at a magnification of 2.5x, as depicted in Figure 2. To analyze the weld bead, the depth of penetration of all weld beads was measured using Image J software in Table 3

2.4.2. Weld width (BW)

The weld beads displayed in Figure 2 were analyzed using Image J software, and the corresponding measurements have been recorded in Table 3.

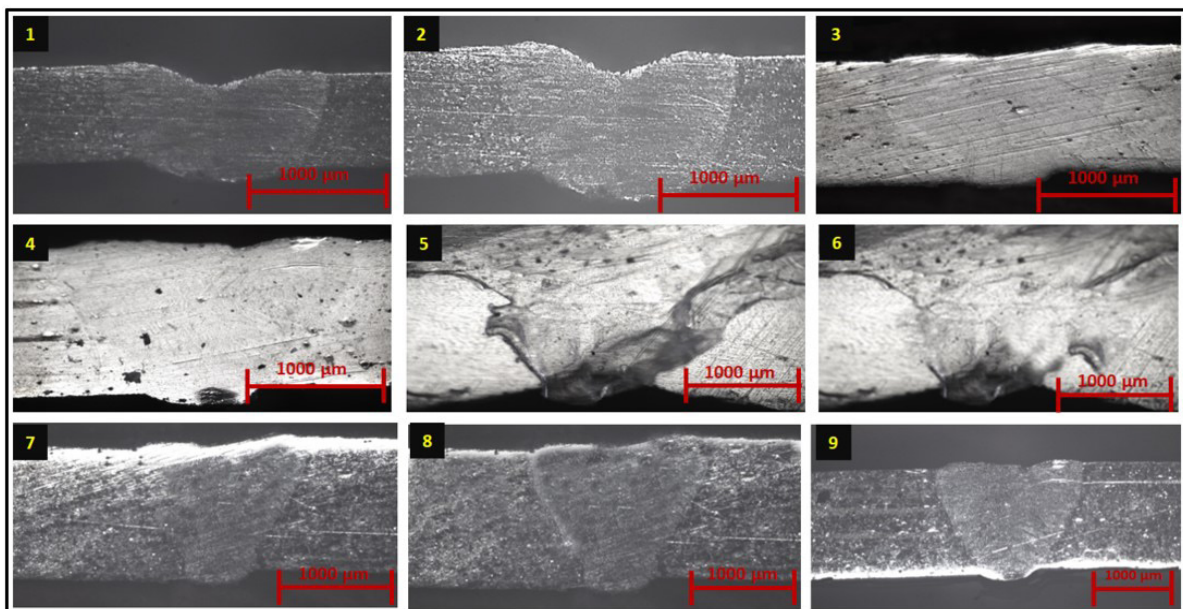


Figure 2. Weld bead geometry. Weld bead macrograph at parameters No 1 to 9

2.4.3. Micro-hardness

The hardness test was conducted in accordance with the ASTM E-384-16 standard [18]. For this study, Vickers hardness measurements were taken along a line passing through the center of the weldments. To determine the hardness of different sections within the weld joint, a 136-degree diamond pyramid indenter was utilized, applying a force of 100g for 15 seconds on the FZ (Fusion Zone), HAZ (Heat-Affected Zone), and BM (Base Metal) respectively. The recorded hardness values are presented in Table 3.

2.4.4. Tensile strength (TS)

The ASTM-E8 standard [10] was followed in the preparation of the tensile test specimens, as shown in Figure 3. A wire-cut electrical discharge machine (WEDM) was used to cut the samples into dog-bone shapes (Figure 4) with gauge lengths of 50 mm and 200 mm overall. To prevent rusting, the samples were adequately cleaned, considering that water is utilized for cooling purposes during the WEDM cutting process. Subsequently, a tensile test was conducted on a Universal Testing Machine (UTM) with a capacity of 100 kN. The test was carried out at a displacement rate of 0.5 mm/min, and the recorded tensile strength results at room temperature are presented in Table 3.

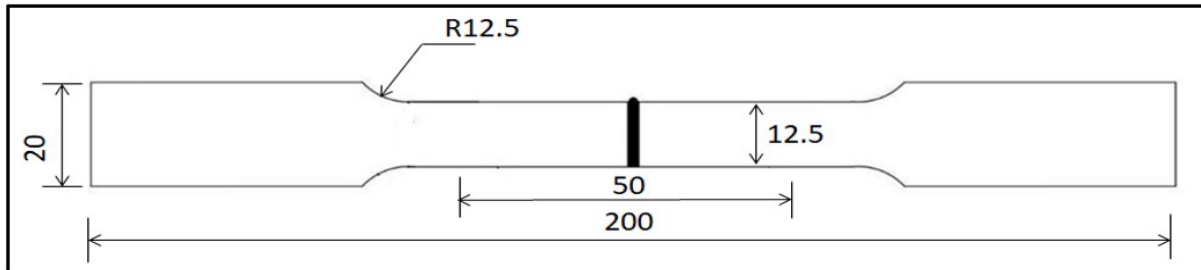


Figure 3. Dimensions of the welded-joint tensile specimen.

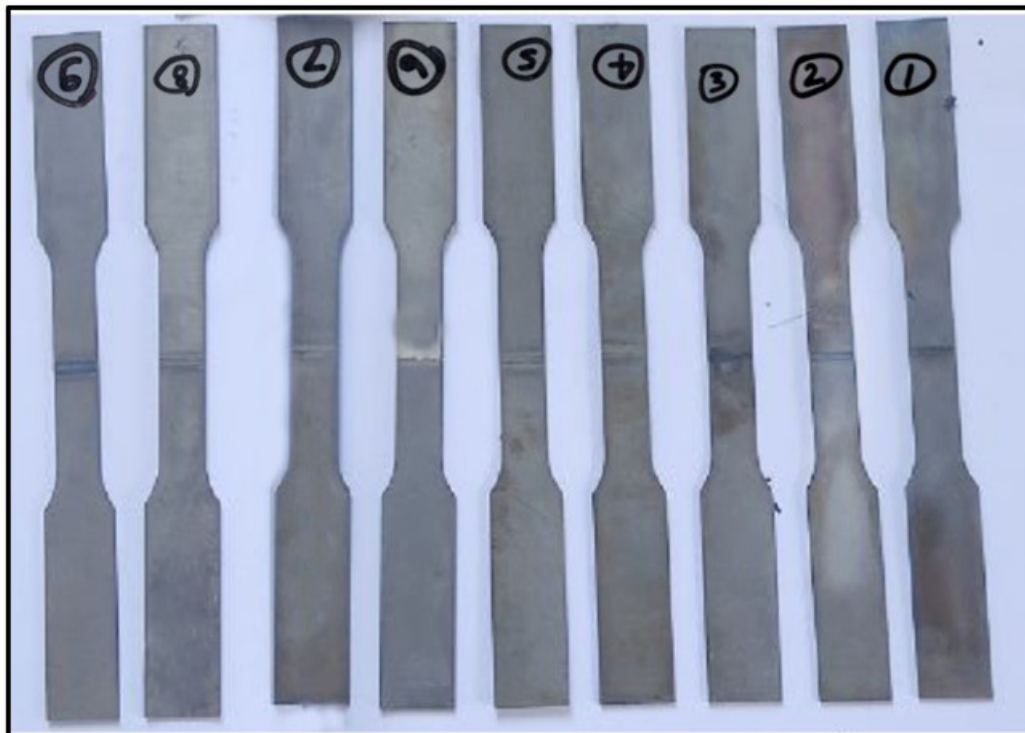


Figure 4. Laser welded tensile joints (set of L_9).

3. Welding Process Optimization Methodology

Two optimization methods: SOO and MOO were used to optimize the process parameters. The design of experiments (DOE) utilizes the Taguchi L_9 orthogonal array, implemented through Minitab statistical software version 20.3. The MOO employs the signal-to-noise (S/N) ratio to determine the optimal combination of individual responses [24,25]. Since Single-optimization does not optimize all process parameters simultaneously. That's why the authors decided to use MOO. Here, Taguchi gray relation analysis (TGRA) coupled with Principal components analysis (PCA) has been used for MOO. The flow chart of welding process optimization for both Single and MOO is in Figure 5.

Based on the type of quality feature, change the actual data from the Taguchi experiment into S/N ratios for response by using the exact formula. S/N ratios are calculated (in Table 3) during experiments based on whether lower is better, higher is better, or nominal is better. The following Equation 1 is used to find out the S/N ratio for higher-is-better [10].

$$\frac{S}{N} \text{ ratio} = -10 \log \left(\frac{1}{n} \sum_{i=1}^n \frac{1}{y_{ij}^2} \right) \quad (1)$$

Here, y_{ij} stands for the i th replica of the j th response, and n stands for the number of replicas. The following Equation 2 is used to find out the S/N ratio for lower-is-better.

$$\frac{S}{N} \text{ ratio} = -10 \log \left(\frac{1}{n} \sum_{i=1}^n y_{ij}^2 \right) \quad (2)$$

3.1. Multi-objective optimization TGRA coupled with PCA

Every response variable in TGRA is allocated identical weights, which might lead to uncertainty in decision-making. As a result, PCA was incorporated to add the relative weight of responses. The following steps were used for TGRA. Expression of Normalisation as shown in Equation 3 and Equation 4.

Larger-the-better

$$y_j^*(k) = \frac{y_j(k) - \min y_j(k)}{\max y_j(k) - \min y_j(k)} \quad (3)$$

Smaller-the-better

$$y_j^*(k) = \frac{\max y_j(k) - y_j(k)}{\max y_j(k) - \min y_j(k)} \quad (4)$$

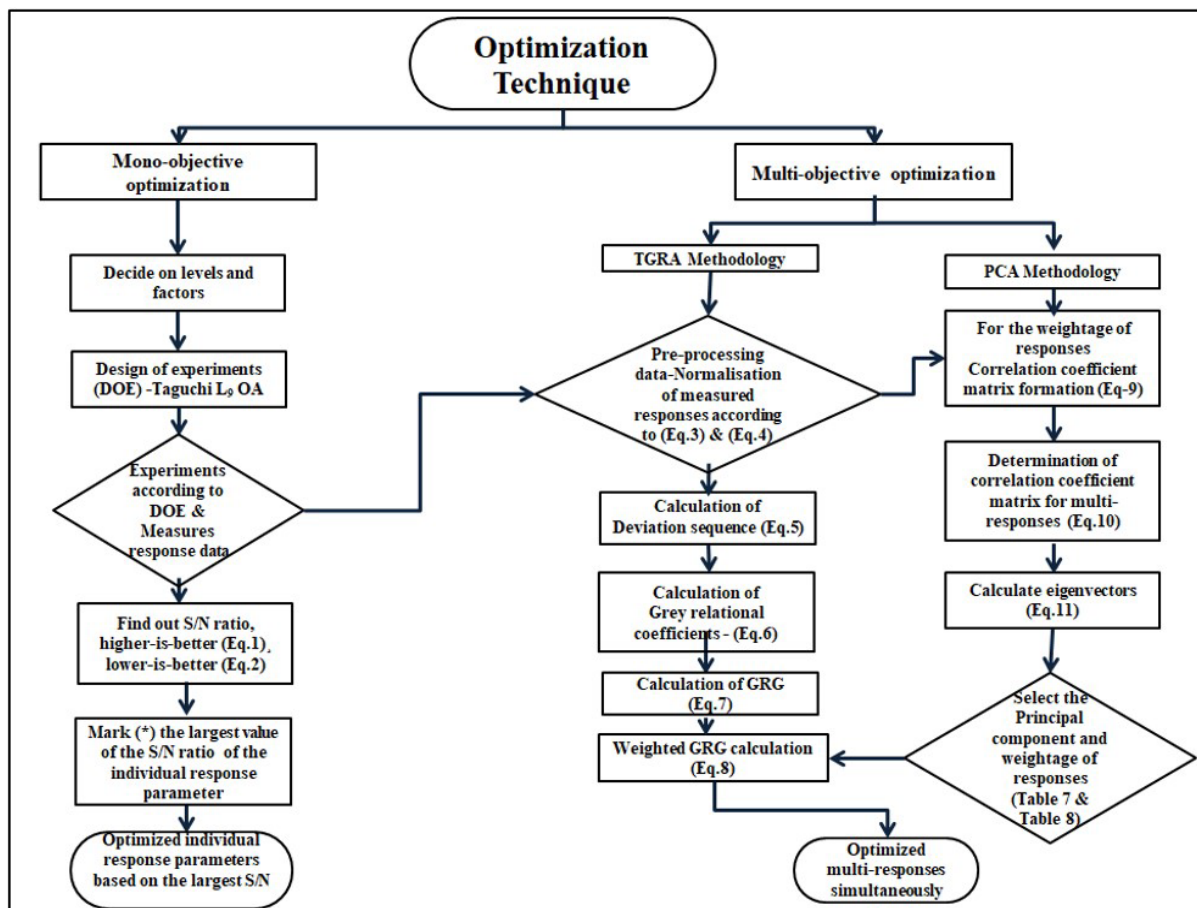


Figure 5. A flow chart of research methodology for MOO. MOO: multi-objective optimisation.

Deviation sequence

$$\Delta_{oi}(k) = |y_0^*(k) - y_j^*(k)| \quad (5)$$

Grey relational coefficients (GRC)

$$\xi \left(y_j^*(k), y_0^*(k) \right) = \frac{\Delta_{min}(k) + \gamma \Delta_{max}(k)}{\Delta_{oi}(k) + \Delta_{max}(k)} \quad (6)$$

Calculation of GRG

$$\gamma_j \left(y_j^*, y_0^* \right) = \frac{1}{n} \sum_{k=1}^n \xi \left(y_j^*(k), y_0^*(k) \right) \quad (7)$$

Weighted GRG calculation

$$\gamma_j \left(y_j^*, y_0^* \right) = \sum_{k=1}^n \omega_k \xi \left(y_j^*(k), y_0^*(k) \right), \text{ where } \sum_{k=1}^n \omega_k = 1 \quad (8)$$

3.2. PCA

PCA is well-established as a highly effective statistical method for accomplishing MOO [26]. It allows for the consolidation of correlated arrays into a smaller set of uncorrelated arrays and principal components, thereby facilitating the optimization process.. Through the utilization of linear combinations, it allows for the exploration of the variance and covariance structure of a defined group [27]. The eigenvalues and eigenvectors were obtained using Equation 9, while the principal components (PCs) were determined using Equation 10. To perform a PCA, several steps need to be followed [26-28].

1. Development of a variance-covariance matrix from data that has been normalized

$$y = \begin{bmatrix} x_{11} & x_{12} & x_{13} & \dots & \dots & x_{1n} \\ x_{21} & x_{22} & x_{23} & \dots & \dots & x_{2n} \\ \dots & \dots & \dots & \dots & \dots & \dots \\ x_{m1} & x_{m2} & x_{m3} & \dots & \dots & x_{mn} \end{bmatrix} \quad (9)$$

Where, m = 9 is no of experiments, n= 4 is no of responses of welded joint

2. Correlation coefficient array is being calculated according to Equation 10

$$R_{jl} = \left(\frac{\text{cov}(x_i(j), x_i(l))}{\sigma_{x_i(j)} \sigma_{x_i(l)}} \right) \quad (10)$$

Where, j = 1, 2, 3....m, i= 1, 2, 3....n

Eigenvalue and eigenvectors were determined by the following Equation 11:

$$(R - \lambda_k I_m) V_{ik} = 0 \quad (11)$$

Where, λ_k eigenvalue, V_{ik} eigenvectors.

3. The principal component is calculated as follows Equation 12:

$$Y_{mk} = \sum_{i=1}^n X_m(i) V_{ik} \quad (12)$$

Where, Y_{mk} principal components (PC), Y_{m1} , Y_{m2} , first PC, second PC, etc.

4. The largest value of PC is considered as the eigenvector that gives the largest variability on the response parameters, the square of the eigenvector was taken as the relative weightage (in Table 8) of response parameters in deciding the MOO of welding quality of weldments.

4. Results and Discussion

4.1. Analysis of experimental data

The collected data from the experiments are analyzed using statistical techniques. Statistical significance tests Probability plots of responses, and analysis of variance (ANOVA) are performed to determine the significance of individual factors and their interactions. The analysis of experimental data provides insights into the main factors influencing welding performance and guides the subsequent analysis and optimization steps.

4.1.1. Probability plots of responses

From the probability plots, it seems that the experimental data is in good agreement with the fitted line and that the normality assumption is reasonable. The Anderson-Darling test is a method used to evaluate how well a set of data fits a particular distribution, such as the normal distribution, and can be used to identify outliers or other deviations from the expected pattern. A low Anderson-Darling statistic value indicates that the data fits the normal distribution well, while a high value suggests that the data deviates significantly from normality. Additionally, a p-value greater than 0.05 suggests that there is not enough evidence to reject the null hypothesis, which in this case would be that the data is normally distributed.

The results presented in Figure 6, indicate that the experimental data for all responses are closely aligned with the fitted line. Additionally, the Anderson-Darling statistics values are relatively low, and the p-values of the test are greater than 0.05. The p-values of all response parameters (BW, DP, HV, and TS) found the greater than 0.05, which are displayed on the graph in Figure 6a-d. Therefore these observations lead us to assume that the data follows a normal distribution. As a result, we can proceed with further analysis and optimization of the data with confidence.

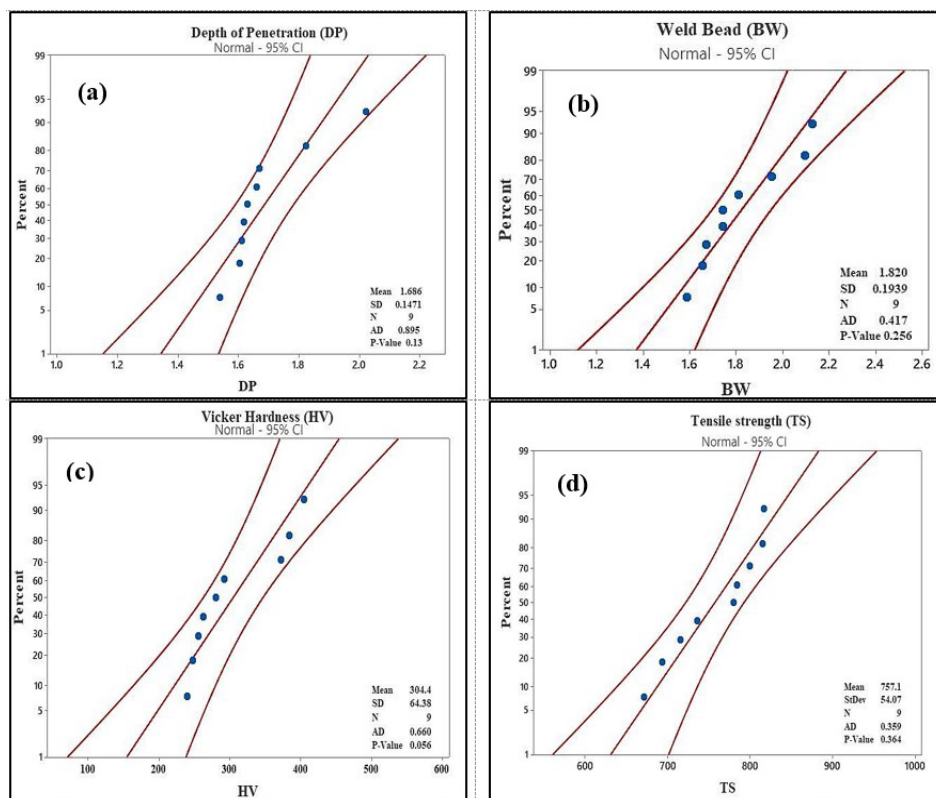


Figure 6. Normal probability plots of responses (a) DP (b) BW (c) HV (d) TS.

4.1.2. Analysis of Variance (ANOVA) for individual responses

To assess the influence of input parameters on each response, we analyzed variance (ANOVA) at a confidence interval of 95%. The ANOVA outcomes for weld bead, depth of penetration, Vickers hardness, and tensile strength can be found in Table 4. A p-value below 0.05 signifies a significant impact of the respective parameter on the response.

Based on the ANOVA results presented in Table 4 and the main effect plot for responses shown in Figure 7a-d, the interpretation of the responses is as follows.

Depth of Penetration- Based on the ANOVA results, it is evident that the WS had the most significant impact, explaining 46% of the observed variation. The laser power had a moderate effect, accounting for 30.58% of the variation. Conversely, the focal distance and gas flow rate had the least impact, contributing to only 11% of the variation in the depth of penetration quality.

The main effect plot in Figure 7a revealed a noteworthy observation: as the WS increases, the depth of penetration decreases, primarily due to the insufficient heating effect on the material. Conversely, the laser power exhibited an optimal value at which the maximum penetration was attained, displaying an initial increase followed by a decrease as the power exceeded that specific value. In contrast, the focal distance and gas flow rate demonstrated minimal influence on the depth of penetration, contributing to a mere 11% of the observed variation. Collectively, these findings emphasize that adjusting the WS and laser power can yield significant effects on the depth of penetration quality in welding, while the impact of focal distance and gas flow rate may be relatively limited.

Table 4. Analysis of variance for individual responses.

Responses	Source	DF	Seq SS	Adj SS	Adj MS	% contribution
Depth of Penetration	p	2	0.052945	0.052945	0.026472	30.58
	v	2	0.079641	0.079641	0.039820	46.00
	f	2	0.020324	0.020324	0.010162	11.74
	g	2	0.020198	0.020198	0.010099	11.68
	Residual Error	0				
	Total	8	0.173108			100
Weld bead	p	2	0.259324	0.259324	0.129662	86.25
	v	2	0.002035	0.002035	0.001017	0.68
	f	2	0.037235	0.037235	0.018617	12.38
	g	2	0.002064	0.002064	0.001032	0.69
	Residual Error	0				
	Total	8	0.300658			100
Vickers Hardness	p	2	30977.6	30977.6	15488.8	93.42
	v	2	713.6	713.6	356.8	2.15
	f	2	686.2	686.2	343.1	2.07
	g	2	782.9	782.9	391.4	2.36
	Residual Error	0				
	Total	8	33160.2			100
Tensile Strength	p	2	10006.9	10006.9	5003.44	42.78
	v	2	3350.2	3350.2	1675.11	14.33
	f	2	6554.9	6554.9	3277.44	28.03
	g	2	3474.9	3474.9	1737.44	14.86
	Residual Error	0				
	Total	8	23386.9			100

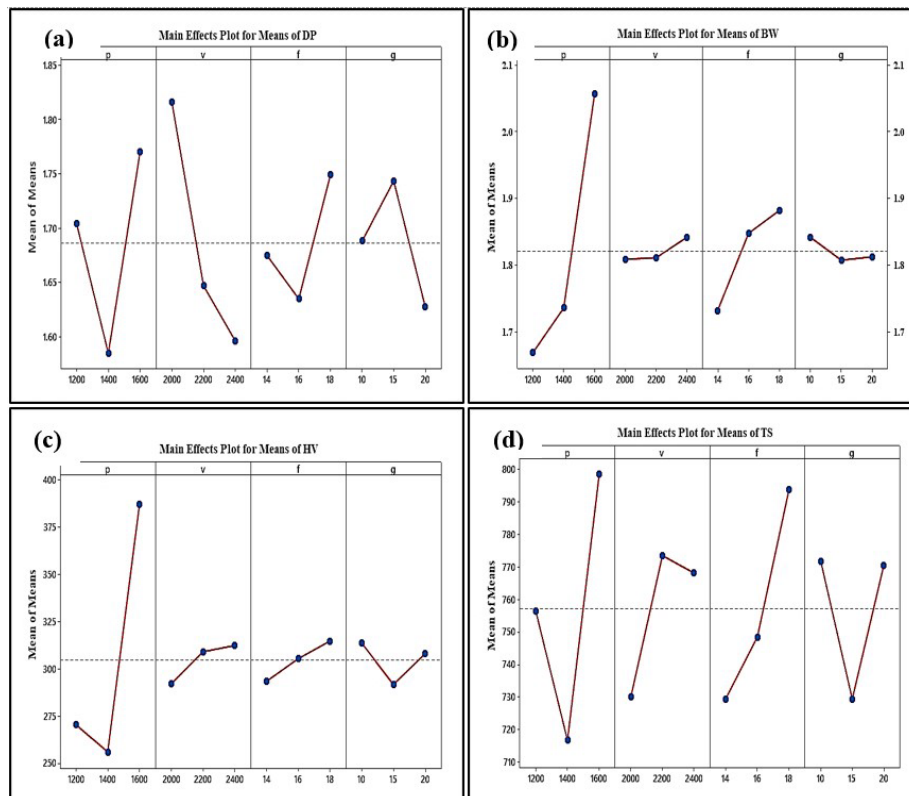


Figure 7. Main effect plots of means for the response variable (a) DP (b) BW (c) HV (d) TS.

Weld bead- Based on the results of ANOVA, it seems that the laser power parameter had the greatest effect on the quality of the weld bead, explaining 86.25% of the observed variation. The focal length parameter had a moderate effect, accounting for 12.38% of the variation, which means that adjusting the focal length can also have a significant impact on the quality of the

weld bead. The findings also indicate that welding velocity and gas flow rate have minor impacts on weld bead quality. Therefore, it is possible that experimenting with these settings may not significantly change the quality of the weld bead.

Weld bead quality improves with both increased laser power and focus distance, as seen in the main effect plot Figure 7b. Because more laser heat is being introduced, weld bead quality can be enhanced by increasing both laser power and focus distance. However, the quality of the weld bead can also be affected by things like the material being welded, the type of laser used, and the welding process.

Vickers Hardness- The results of an ANOVA analysis addressed the relationship between the Vickers micro-hardness value and the variables of LP, WS, FD, and GR. The results show that the LP is the most influential factor in determining the micro-hardness quality, affecting 46% of the observed variation.

Furthermore, the main effect plot Figure 7c demonstrates that as LP was raised, the microhardness initially declined and subsequently increased. This is probably because of the microstructural changes brought on by the heating process. However, WS, FD, and gas flow rate accounted for just 2% of the variation in microhardness quality. Taken together, these findings point to LP as the primary determinant of Vickers microhardness quality in this experiment.

Tensile Strength- According to the analysis of variance (ANOVA) outcomes, it is evident that the LP and focal length variables exhibit the highest level of significance in relation to the weld joint's strength. By augmenting the LP and adjusting the focal length, the weld strength can be enhanced until reaching a specific threshold, beyond which it begins to deteriorate. This implies that the optimisation of LP and focal length configurations can yield optimal outcomes in terms of weld strength. Nevertheless, it is imperative to take into account additional variables including the weldment's constituent material, the specific laser employed, and the chosen welding methodology, as these factors can exert influence on the resultant weld integrity.

The main effect plot in Figure 7d shows how laser parameters affect weld strength. The plot shows that laser power initially increases weld strength, but beyond a threshold, it decreases. Weld strength increases with focal length. This information can be used to alter LP and focus length for weld strength. In conclusion, the ANOVA and main effect plot reveal weld joint quality parameters. These discoveries can optimize welding and improve weld quality and reliability. Overall, the ANOVA and main effect plot reveal weld joint quality parameters. These discoveries can optimize welding and increase weld quality and reliability.

4.2. Single-objective optimization

Single-objective optimization is predicated on the Signal-to-Noise (S/N) ratio. Table 5 displays the S/N ratio for each level of the investigated factor or variable, which indicates the relationship between what is needed response (signal) and the fluctuation or undesired response (noise). The individual responses analyzed in this research present conflicting objective functions, as the aim is to maximize tensile strength, micro-hardness, and depth of penetration, while simultaneously minimizing weld width. To provide clarity, we can reframe these objectives in terms of maximizing the signal and minimizing the noise. The signal, in this context, encompasses the desired outcomes such as high tensile strength, micro-hardness, and depth of penetration, while the noise refers to the undesired consequence of a wide weld. Consequently, the primary objective of this study is to optimize the signal-to-noise ratio by enhancing the signal components (tensile strength, micro-hardness, and depth of penetration) and minimizing the noise component (weld width).

Table 5. S/N of response parameters.

Exp No.	S/N ratio of Responses			
	DP	BW	HV	TS
1	-4.02248*	5.220497	48.1648	57.09826
2	-4.46992	4.454329	48.39911	57.33756
3	-4.82595	4.17957	49.30766	58.24444*
4	-4.82595	4.104087	47.88903	56.82719
5	-5.14877	4.136518	48.94316	57.88632
6	-4.37596	3.750414	47.60422	56.54739
7	-6.41953	6.107027*	51.41086	57.84189
8	-5.80515	4.402162	51.68662	58.0618
9	-6.55535	4.243752	52.1491*	58.22315
Optimum*	p₁-V₁-f₁-g₁	p₃-V₁-f₃-g₂	p₃-V₃-f₂-g₁	p₁-V₃-f₃-g₃

* In bold font optimized setting of individual responses for Single-optimization.

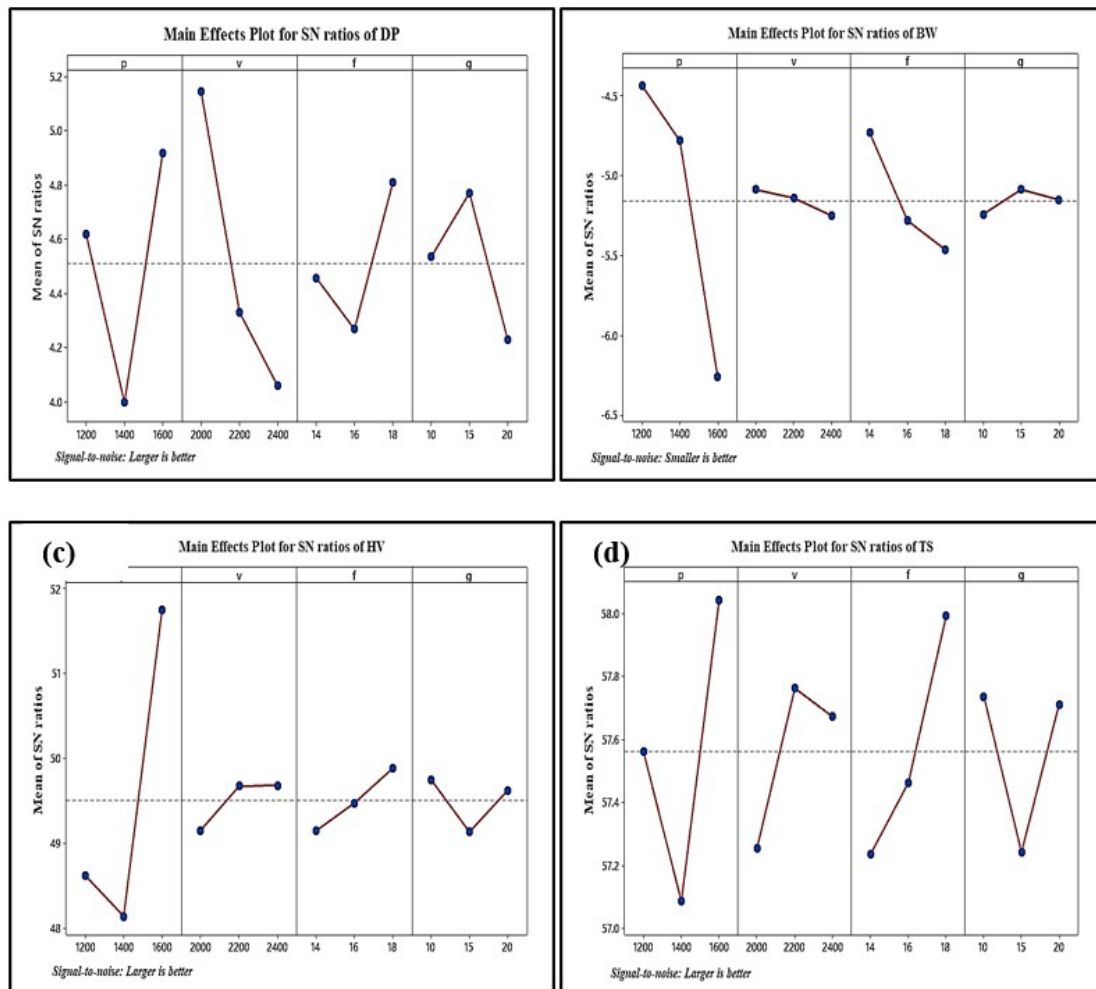


Figure 8. Main effects plots of the S/N ratio for the response variable (a) DP (b) BW (c) HV (d) TS.

To determine the optimal level of the factor, the S/N ratios are calculated for each level, and the average S/N ratio for each level is computed. The level with the highest average S/N ratio is considered the optimal level because it indicates the level at which the desired response is most distinguishable from the noise. In general, higher S/N ratios indicate better quality characteristics, as they indicate a stronger signal relative to the noise. Therefore, identifying the level with the highest average S/N ratio can help identify the optimal level for achieving the desired response with the highest possible quality. From the S/N ratio Table 5, shows that the highest signal-to-noise (S/N) ratio of 6.10 was obtained for weld width (BW) at experimental run 7, where laser power was at level 3, welding speed was at level 1, FD was at level 3, and gas flow rate was at level 2. This indicates that these specific parameter settings resulted in the most desirable outcome for weld width. Similarly, for depth of penetration, micro-hardness, and tensile strength, the highest S/N ratios were obtained for experimental sets $p_1-v_1-f_1-g_1$, $p_3-v_3-f_2-g_1$, and $p_1-v_3-f_3-g_3$, respectively. This means that these specific combinations of parameter settings resulted in the most desirable outcomes for each of these metrics.

Based on Table 5 and the Main effects plots of the S/N ratio (Figure 8), there is a significant inconsistency among the quality responses of the system being studied. This indicates that optimizing a single parameter may not necessarily lead to an optimal solution that satisfies all the responses simultaneously. In such cases, it is advisable to use MOO techniques to identify an optimal setting that simultaneously satisfies all the responses.

4.3. Multi-objective Optimization (MOO) of response parameters

The technique of MOO is employed to simultaneously optimize multiple objectives. The primary aim of MOO is to discover a set of solutions that strikes the optimal balance among the various objectives. In this research paper, the method of MOO encompasses the coupling of TGRA (Taguchi gray relation analysis) with PCA (Principal Component Analysis). By leveraging PCA to identify the most significant objectives, TGRA directs its optimization endeavors towards these specific objectives, resulting in a streamlined and highly efficient optimization process. The normalized value of the output parameter in Table 6 and their TGRA in Table 7 are calculated to obtain MOO.

Table 6. Normalization of response parameters and their deviation.

Exp. No	Normalized value, $y_j^*(k)$				Deviation sequence, $\Delta_{\sigma_j}(k)$			
	DP	BW	HV	TS	DP	BW	HV	TS
1	0.592	1.000	0.303	0.097	0.408	0.000	0.697	0.903
2	0.271	0.844	0.441	0.139	0.729	0.156	0.559	0.861
3	0.163	0.714	1.000	0.315	0.838	0.286	0.000	0.685
4	0.133	0.714	0.152	0.048	0.867	0.286	0.848	0.952
5	0.146	0.591	0.772	0.242	0.854	0.409	0.228	0.758
6	0.000	0.877	0.000	0.000	1.000	0.123	1.000	1.000
7	1.000	0.061	0.745	0.800	0.000	0.939	0.255	0.200
8	0.250	0.327	0.883	0.873	0.750	0.673	0.117	0.127
9	0.188	0.000	0.986	1.000	0.813	1.000	0.014	0.000

Table 7. Taguchi Gray relation coefficient (TGRC).

Exp. No	Gray relation coefficient				TGRG	Rank	W-TGRG	W-Rank
	DP	BW	HV	TS				
1	0.355	0.500	0.295	0.263	0.3531	5	0.3453	5
2	0.289	0.432	0.321	0.269	0.3278	7	0.3335	7
3	0.272	0.389	0.500	0.297	0.3644	4	0.3844	3
4	0.268	0.389	0.271	0.256	0.2958	9	0.3002	9
5	0.270	0.355	0.407	0.284	0.3291	6	0.3419	6
6	0.250	0.445	0.250	0.250	0.2988	8	0.3080	8
7	0.500	0.258	0.398	0.417	0.3932	1	0.3663	4
8	0.286	0.299	0.448	0.444	0.3689	3	0.3975	2
9	0.276	0.250	0.493	0.500	0.3798	2	0.4177	1

4.4. PCA

PCA determines the relative importance or weight of different quality responses [29]. Eigenvalues and eigenvectors are important components of PCA, and they are often used to calculate the principal components, which are linear combinations of the original variables that capture the most variation in the data. The results of this analysis are presented in Table 8 and Table 9. The percentage of total variation described by each primary component was utilized as a priority weight value to assign relative importance to the quality responses. To clarify, the first principal component (PC)'s eigenvector is used to calculate the relative weights for the quality replies [30]. This PC explained the most variation.

Table 8. Calculation of Eigenvalue and Proportion for PCs.

PCs	Eigenvalue	Proportion	Cumulative
First	0.021849	0.691	0.691
Second	0.006329	0.200	0.892
Third	0.002484	0.079	0.970
Fourth	0.000944	0.030	1.000

Table 9. Calculation of the value of Eigenvectors for PCs.

Response Parameters	Eigenvectors			
	PC1	PC2	PC3	PC4
DP	0.164	-0.895	0.415	0.019
BW	-0.545	0.087	0.369	0.748
HV	0.548	0.432	0.716	-0.004
TS	0.613	-0.07	-0.423	0.664

In order to calculate the relative weights of every performance response, the eigenvectors of the first principal components were squared. This means that the squared values of the eigenvectors were used as relative weight of response parameter. The authors found the relative importance of each component in explaining the variance of the data [31] are 0.0269, 0.2970, 0.3003, and 0.3758 for DP, BW, HV, and TS, respectively, as shown in Table 10.

Table 10. Calculation of every response parameter's contribution to the principal component.

Response parameters	Contributions/weightage	Percentage contribution (%)
Depth of penetration (DP)	0.0269	2.69
Bead width (BW)	0.2970	29.70
Hardness (HV)	0.3003	30.03
Tensile strength (TS)	0.3758	37.58

Table 11. Response table of Means (average) of W-TGRG.

Level	1	2	3	Delta	Rank
p	0.3544	0.3167	0.3938	0.0771	1
v	0.3373	0.3576	0.3700	0.0328	2
f	0.3503	0.3505	0.3642	0.0139	4
g	0.3683	0.3359	0.3607	0.0324	3

Bold font of Table 11. represent the multi-objective (TGRA integrated with PCA) set of optimized parameters. The ANOVA analysis of means evaluates the percentage contribution of these optimal parameters within the context of MOO. The obtained Multi-objective optimal setting is $p_3-v_3-f_3-g_1$.

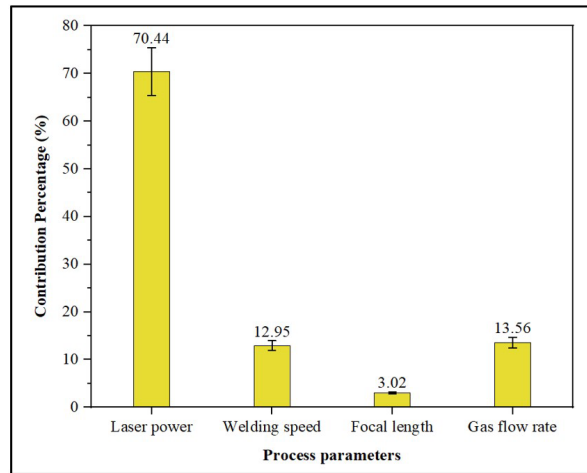


Figure 9. Contributions of process parameters on the multi-objective optimized responses.

Based on the ANOVA analysis of means in the context of MOO, it was observed that laser power had the most substantial impact, accounting for 70.44% of the observed variation (in Figure 9). WS and GR exhibited moderate effects, contributing approximately 13% each. Conversely, the FD had the least influence, with a minimal effect of 3% on the MOO of responses in laser welding.

4.5. Confirmation experiment

A confirmation experiment (in Table 12) is a scientific experiment that is conducted to confirm or verify the results of a previous study. The purpose of a confirmation experiment is to ensure that the original results were not due to chance or some other confounding factor. The authors have conducted experiments using the optimal setting ($p_3-v_3-f_3-g_1$) to confirm the adequacy of using the TGRA-PCA methodology in the laser welding process and compared the results against the results obtained using ($p_1-v_1-f_1-g_1$). The authors found an improvement in DP, BW, HV, and TS by 6.03%, 8.74%, 12.5%, and 16.48% respectively. These results suggest that the GRA-PCA methodology is effective in optimizing the laser welding process, as it led to significant improvements in multiple performance metrics. Overall, the conclusion drawn by the authors is that the TGRA-PCA methodology is adequate for use in MOO of the laser welding process, as it yielded improved results in comparison to the initial values.

Table 12. Summary of confirmation experiments using TGRA coupled with PCA.

Output parameters	Initial setting $p_1-v_1-f_1-g_1$	Optimal setting $p_3-v_3-f_3-g_1$	Improvement (%)
Depth of penetration	1.824	1.934	6.03
Weld width	1.589	1.450	8.74
Vickers hardness	256	288	12.5
Tensile strength	716	834	16.48

4.6. Macrostructural and microstructural characterization

An optical microscope (OM) was used to examine the macrostructure of the weld bead, the microstructure of the base metal (BM), fusion zone (FZ), heat-affected zone (HAZ), and WM/HAZ interface. Samples of the required size for BM, FZ, HAZ,

and FZ/HAZ interface were sectioned and mounted. The metallographic samples were prepared according to standard procedures, which involved grinding with silicon carbide emery paper of grit sizes 100 and 2000, polishing, and etching with a solution of 15 ml HCL, 10 ml CH₃COOH, 5 ml HNO₃ and 2 drops glycerol. Polished samples were dipped into etchant for 12 s, and after this washed with distilled water and dried with an air dryer before examining the microscope.

An optical image was captured to analyze the macro and microstructure of the welded joint, as depicted in Figure 10a-c. The image displays the presence of a twin boundary structure, which has been encircled in yellow illustrated in Figure 10a. This twin boundary structure is a result of the recrystallization process that took place in the Nimonic 80A sheet, which was subjected to temperatures above 950 °C [32,33].

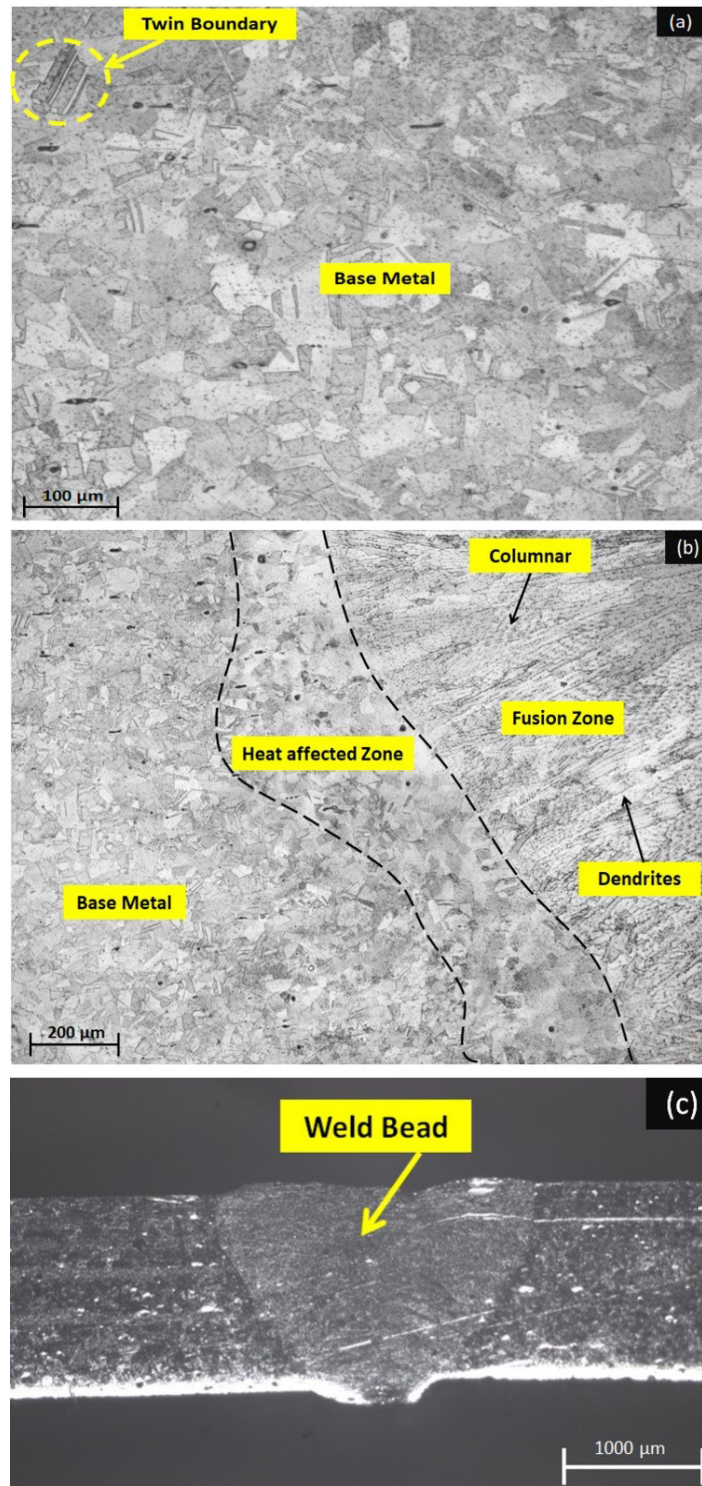


Figure 10. Optical image at optimum parameter (a) Base metal (b) integral microscopy of BM, HAZ, and FZ (c) weld Bead.

It should be noted that the formation of twin boundaries in the metal sheet is a direct consequence of this recrystallization process. The microstructure of the weldments showed changes, as evident from Figure 10a, b. Optical image of weldments of CO_2 laser beam welding was revealed dendrites in fusion zone, dendrites grow in a columnar manner at the fusion line, which eventually turn into partially needle-shaped equiaxed grains. The fast cooling associated with laser beam welding leads to the formation of a dendrites structure in the fusion zones [34]. The base metal contains a gamma phase (γ) and metal carbide (MC) at the grain boundary. Similar observations were made by Subramani in GTAW [35]. The macrostructural image of the weld metal cross-section (weld bead) at the optimal set of multi-objective parameters is depicted in Figure 10c.

5. Conclusion

In this paper, The Taguchi L_9 OA approach combined with the GRA called TGRA coupled with PCA method was found to be effective for solving the complicated MOO problem related to laser welding quality-response parametric optimization. The weightage for quality responses that influence GRGs was successfully extracted using PCA, which helped in identifying the optimal solution. In the context of optimal settings, confirmatory experiments could be conducted to cross-check the findings of previous studies that have identified an optimal setting for a particular task or process. The present research provides the following valuable insights for improving the quality and efficiency of CO_2 laser welding processes.

1. The tensile strength and microhardness value of the welded joint were found to be less as compared to base metal because the dendrite's microstructure in the fusion zone and columnar in the heat-affected zone are present;
2. It is observed that there are changes in microstructure in the fusion zone and heat-affected zone of welded joint as that of base metal;
3. The experimental data exhibits strong concurrence with the fitted line, follow assumption of its normal distribution. Science a p-value exceeding 0.05, indicating a lack of substantial evidence to reject the null hypothesis, which emphasizes the data are a normal distribution. From ANOVA analysis, the results indicate that laser power has the greatest influence on both Vickers hardness and tensile strength of the weld bead. On the other hand, welding speed exhibits the most significant effect on the depth of penetration;
4. MOO optimizes the individual welding responses independently. The individual optimal set (Single optimal setting) of welding parameters for each welding response were found. These found sets are for high tensile strength, depth of penetration, microhardness $p_1-v_3-f_3-g_3$, $p_1-v_1-f_1-g_1$, $p_3-v_3-f_2-g_1$, and for low weld bead, $p_3-v_1-f_3-g_2$ respectively;
5. The multi-optimal set of parameters is $p_3-v_3-f_3-g_1$ for the combination of TGRA with PCA for CO_2 laser welding processes on superalloy 80A. The percentage contributions obtained with the help of the PCA analysis of each quality response variable, were 2.69%, 29.70%, 30.03%, and 37.58% for DP, BW, HV, and TS, respectively. It indicates the relative importance of each component on the weld joint simultaneously. Tensile strength and hardness have high impact;
6. Confirmation of the experiments based on W- TGRA show that Depth of penetration is 6.03%, weld bead 8.74%, Vickers hardness 12.5% and tensile strength 16.48% respectively, which confirm the adequacy of used TGRA coupled with PCA for MOO.

The findings of the research work can serve as guidelines and standards for the CO_2 laser welding in practical applications. Additionally, further research should focus on investigating the impact of both quantitative and qualitative inputs on other outputs, including but not limited to bead reinforcement, Impact energy, and residual stresses. Ultimately, it was determined that the Weighted Taguchi Grey Relational Analysis (W-TGRA) algorithm is a straightforward, effective, and efficient tool for stakeholders in the welding industry.

Authors' contributions

Suman Kumar Saurabh, Prabha Chand, Umacharan Singh Yadav: conceptualization and methodology. Suman Kumar Saurabh: data curation, writing - original draft preparation. Suman Kumar Saurabh, Prabha Chand Umacharan Singh Yadav: critical revision, investigation and validation.

Statements and declarations

In this article, All data generated or analyzed during this investigation are accessible to the author upon reasonable request.

Acknowledgements

The Authors express their gratitude to Magod Laser, Bengaluru, India, a renowned leader in laser manufacturing for providing support in conducting experimental work. Additionally, the Authors extend their thanks to NIT Jamshedpur for facilitating the OM and Microhardness tests, and to IIT (ISM) Dhanbad for conducting the tensile test.

References

- [1] Das D, Jaypuria S, Pratihari DK, Roy GG. Weld optimization. *Science and Technology of Welding and Joining*. 2021;26(3):181-195. <http://dx.doi.org/10.1080/13621718.2021.1872856>.
- [2] Huang Q, Hagstrom J, Skoog H, Kullberg G. Effect of CO₂ laser parameter variations on sheet metal welding. *International Journal for the Joining of Materials*. 1991;3(3):79-88.
- [3] Pankaj P, Tiwari A, Bhadra R, Biswas P. Experimental investigation on CO₂ laser butt welding of AISI 304 stainless steel and mild steel thin sheets. *Optics & Laser Technology*. 2019;119:105633. <http://dx.doi.org/10.1016/j.optlastec.2019.105633>.
- [4] Smith RJ, Lewi GJ, Yates DH. Development and application of nickel alloys in aerospace engineering. *Aircraft Engineering*. 2001;73(2):138-147. <http://dx.doi.org/10.1108/00022660110694995>.
- [5] Kim DK, Kim DY, Ryu SH, Kim DJ. Application of nimonic 80A to the hot forging of an exhaust valve head. *Journal of Materials Processing Technology*. 2001;113(1-3):148-152. [http://dx.doi.org/10.1016/S0924-0136\(01\)00700-2](http://dx.doi.org/10.1016/S0924-0136(01)00700-2).
- [6] Subramani P, Manikandan M. Development of welding technique to suppress the microsegregation in the aerospace grade alloy 80A by conventional current pulsing technique. *Journal of Manufacturing Processes*. 2018;34:579-592. <http://dx.doi.org/10.1016/j.jmapro.2018.06.037>.
- [7] Ancona A, Sibillano T, Tricarico L, Spina R, Lugara PM, Basile G, et al. Comparison of two different nozzles for laser beam welding of AA5083 aluminium alloy. *Journal of Materials Processing Technology*. 2005;164:971-977. <http://dx.doi.org/10.1016/j.jmatprotec.2005.02.048>.
- [8] Benyounis KY, Olabi AG, Hashmi MSJ. Multiresponse optimization of CO₂ laser-welding process of austenitic stainless steel. *Optics & Laser Technology*. 2008;40(1):76-87. <http://dx.doi.org/10.1016/j.optlastec.2007.03.009>.
- [9] Moradi M, Ghoreishi M. Influences of laser welding parameters on the geometric profile of Ni-base superalloy Rene 80 weld-bead. *International Journal of Advanced Manufacturing Technology*. 2011;55(1-4):205-215. <http://dx.doi.org/10.1007/s00170-010-3036-1>.
- [10] Padmanaban G, Balasubramanian V. Optimization of laser beam welding process parameters to attain maximum tensile strength in AZ31B magnesium alloy. *Optics & Laser Technology*. 2010;42(8):1253-1260. <http://dx.doi.org/10.1016/j.optlastec.2010.03.019>.
- [11] Sathiyaraj P, Abdul Jaleel MY, Katherasan D, Shanmugarajan B. Optimization of laser butt welding parameters with multiple performance characteristics. *Optics & Laser Technology*. 2011;43(3):660-673. <http://dx.doi.org/10.1016/j.optlastec.2010.09.007>.
- [12] Benyounis KY, Olabi AG, Hashmi MS. Multi-response optimization of CO₂ laser-welding process of austenitic stainless steel. *Optics & Laser Technology*. 2008;40(1):76-87. <http://dx.doi.org/10.1016/j.optlastec.2007.03.009>.
- [13] Park H, Rhee S. Estimation of weld bead size in CO₂ laser welding by using multiple regression and neural network. *Journal of Laser Applications*. 1999;11(3):143-150. <http://dx.doi.org/10.2351/1.521890>.
- [14] Anawa EM, Olabi AG. Using Taguchi method to optimize welding pool of dissimilar laser-welded components. *Optics & Laser Technology*. 2008;40(2):379-388. <http://dx.doi.org/10.1016/j.optlastec.2007.07.001>.
- [15] Choudhury B, Singh V, Singh AP, Chandrasekaran M, Patel Y, Singh SK. Simultaneous optimization of weld bead geometry and weld strength during gas tungsten arc welding of Inconel 825 strips using desirability function coupled with grey relational analysis (DF-GRA). *Engineering Research Express*. 2023;5(1):015035. <http://dx.doi.org/10.1088/2631-8695/acbbba>.
- [16] Davim JP, editor. *Statistical and computational techniques in manufacturing*. USA: Springer Science & Business Media; 2012. <http://dx.doi.org/10.1007/978-3-642-25859-6>.
- [17] Krishnan M, Subramaniam S. Multi-response optimization of friction stir corner welding of dissimilar thickness AA5086 and AA6061 aluminum alloys by Taguchi grey relational analysis. *Proceedings of the Institution of Mechanical Engineers. Part C, Journal of Mechanical Engineering Science*. 2019;233(11):3733-3742. <http://dx.doi.org/10.1177/0954406218806032>.
- [18] Sarkar A, Majumder A, Pawar M, Saha SC, Rai RN. Optimization of process parameters of submerged arc welding by using grey-fuzzy-based Taguchi method for AISI 1518 grade steel. *Proceedings of the Institution of Mechanical Engineers. Part B, Journal of Engineering Manufacture*. 2014;228(11):1491-1500. <http://dx.doi.org/10.1177/0954405414521064>.
- [19] Sameer MD, Birru AK. Optimization and characterization of dissimilar friction stir welded DP600 dual phase steel and AA6082-T6 aluminium alloy sheets using TOPSIS and grey relational analysis. *Materials Research Express*. 2019;6(5):056542. <http://dx.doi.org/10.1088/2053-1591/aafba4>.
- [20] Nguyen PH, Banh TL, Mashood KA, Tran DQ, Dong Pham V, Muthuramalingam T, et al. Application of TGRA-based optimisation for machinability of high-chromium tool steel in the EDM process. *Arabian Journal for Science and Engineering*. 2020;45(7):5555-5562. <http://dx.doi.org/10.1007/s13369-020-04456-z>.
- [21] Payal H, Maheshwari S, Bharti PS. Parametric optimization of EDM process for Inconel 825 using GRA and PCA approach. *Journal of Information and Optimization Sciences*. 2019;40(2):291-307. <http://dx.doi.org/10.1080/02522667.2019.1578090>.

- [22] Abas M, Naeem K, Habib T, Khan I, Farooq U, Khalid QS, et al. Development of prediction model for conductive pattern lines generated through positive displacement microdispensing system using artificial neural network. *Arabian Journal for Science and Engineering*. 2021;46(3):2429-2442. <http://dx.doi.org/10.1007/s13369-020-05103-3>.
- [23] Sharma SK, Maheshwari S. Multi-objective optimization of HAZ characteristics for submerged arc welding of micro-alloyed high strength pipeline steel using GRA-PCA approach. *Journal for Manufacturing Science and Production*. 2016;16(4):263-271. <http://dx.doi.org/10.1515/jmsp-2016-0027>.
- [24] Kurt HI, Oduncuoglu M, Yilmaz NF, Ergul E, Asmatulu R. A comparative study on the effect of welding parameters of austenitic stainless steels using artificial neural network and Taguchi approaches with ANOVA analysis. *Metals*. 2018;8(5):326. <http://dx.doi.org/10.3390/met8050326>.
- [25] Umair M, Shaker K, Ahmad N, Hussain M, Jabbar M, Nawab Y. Simultaneous optimization of woven fabric properties using principal component analysis. *Journal of Natural Fibers*. 2017;14(6):846-857. <http://dx.doi.org/10.1080/15440478.2017.1279994>.
- [26] Siddiquee AN, Khan ZA, Mallick Z. Grey relational analysis coupled with principal component analysis for optimization design of the process parameters in in-feed centreless cylindrical grinding. *International Journal of Advanced Manufacturing Technology*. 2010;46(9-12):983-992. <http://dx.doi.org/10.1007/s00170-009-2159-8>.
- [27] Yadav US, Yadava V. Modelling and optimization of process parameters of electrical discharge diamond drilling of nimonic alloy-an aerospace material. *International Journal of Industrial and Systems Engineering*. 2018;29(4):507-532. <http://dx.doi.org/10.1504/IJISE.2018.094270>.
- [28] Das R, Ball AK, Roy SS. Application of PCA-based hybrid methodologies for parameter optimization of E-jet based micro-fabrication process: a comparative study. *Journal of the Brazilian Society of Mechanical Sciences and Engineering*. 2018;40(9):1-3. <http://dx.doi.org/10.1007/s40430-018-1373-4>.
- [29] Qazi MI, Akhtar R, Abas M, Khalid QS, Babar AR, Pruncu CI. An integrated approach of GRA coupled with principal component analysis for multi-optimization of shielded metal arc welding (SMAW) process. *Materials (Basel)*. 2020;13(16):3457. <http://dx.doi.org/10.3390/ma13163457>. PMID:32764439.
- [30] Qazi MI, Abas M, Khan R, Saleem W, Pruncu CI, Omair M. Experimental investigation and multi-response optimization of machinability of AA5005H34 using composite desirability coupled with PCA. *Metals*. 2021;11(2):235. <http://dx.doi.org/10.3390/met11020235>.
- [31] David SA, Babu SS, Vitek JM. Welding: solidification and microstructure. *Journal of the Minerals Metals & Materials Society*. 2003;55(6):14-20. <http://dx.doi.org/10.1007/s11837-003-0134-7>.
- [32] Pérez M. Microstructural evolution of Nimonic 80a during hot forging under non-isothermal conditions of screw press. *Journal of Materials Processing Technology*. 2018;252:45-57. <http://dx.doi.org/10.1016/j.jmatprotec.2017.09.014>.
- [33] Lippold JC. *Welding metallurgy and weldability*. Hoboken: John Wiley & Sons; 2014.
- [34] Celen S, Karadeniz S, Özden H. Effect of laser welding parameters on fusion zone morphological, mechanical and microstructural characteristics of AISI 304 stainless steel. *Materialwissenschaft und Werkstofftechnik*. 2008;39(11):845-850. <https://doi.org/10.1002/mawe.200800384>.
- [35] Arivarasu M, Roshith P, Padmanaban R, Thirumalini SKV, Phani Prabhakar KV, Padmanabham G. Investigations on metallurgical and mechanical properties of CO₂ laser beam welded Alloy 825. *Canadian Metallurgical Quarterly*. 2017;56(2):232-244. <http://dx.doi.org/10.1080/00084433.2017.1315847>.